A cubic coordination framework constructed from benzobistriazolate ligands and zinc ions having selective gas sorption properties†

Shyam Biswas,[a] Maciej Grzywa,[a] Hari Pada Nayek,[b] Stefanie Dehnen,[b] Irena Senkovska,[c] Stefan Kaskel[c] and Dirk Volkmer*[a]

Two novel metal coordination polymers, $[Zn_5Cl_4(BBTA)_3]\cdot 3$ DMF (**1**), and $[ZnCl(BBTA)_{0.5}(DMA)]$ (**2**) {H_2-BBTA = 1H,5H-benzo(1,2-d:4,5-d′)bistriazole}, have been synthesized under solvothermal conditions using $ZnCl_2$ and H_2-BBTA in DMF (DMF = *N*,*N*′-dimethylformamide) or DMA (DMA = *N*,*N*′-dimethylacetamide). Moreover, a highly efficient microwave synthetic route has been developed for **1**. The structures of both compounds have been determined by single crystal X-ray diffraction. Compound **1** represents the first example of a novel family of cubic microporous metal–organic frameworks (MFU-4; *M*etal-Organic *F*ramework *U*lm University-4), consisting of dianionic $BBTA^{2-}$ linkers and pentanuclear $\{Zn_5Cl_4\}^{6+}$ secondary building units, whereas compound **2** forms a dense 2D layered framework. Phase purity of both compounds was confirmed by X-ray powder diffraction (XRPD), IR spectroscopy, and elemental analysis. TGA and variable temperature XRPD (VTXRPD) experiments carried out on **1** indicate that solvent molecules occluded in the large cavities of **1** can be removed at a temperature >250 °C in high vacuum without significant loss of crystallinity, giving rise to a metal–organic framework with void cavities. Due to the small diameter of the aperture joining the two types of cavities present in **1**, the diffusion of guest molecules across the crystal lattice is largely restricted at ambient conditions. Compound **1** therefore exhibits a highly selective adsorption for hydrogen *vs.* nitrogen at −196 °C. The framework is stable against moisture and has a specific pore volume of 0.42 $cm^3\ g^{-1}$ estimated from the water adsorption isotherm.

Introduction

Research activity on metal-coordination polymers has undergone a renaissance in recent years.[1] Typically, organic linkers are used in conjunction with metal ions having preferential coordination numbers and geometries, which provides a degree of control over the final structure. Porous coordination polymers, which are now frequently referred to as metal–organic frameworks (MOFs), contain well-defined pores and cavities, similar to zeolites, rendering them interesting candidates for a host of applications, where porosity characteristics is combined with diverse functions such as magnetic,[2] optical,[3] storage,[4] separation,[5] ion-exchange,[6] or catalytic properties.[7] While many MOFs so far have been synthesized using 3d transition metal ions and multidentate arylcarboxylate[8] ligands, there are very few examples on MOFs that contain exclusively N-donor ligands such as 4,4′-bipyridines,[9] pyrazolates,[10] 1,2,4-triazolates,[11] or tetrazolates.[12] Though there are few reports of coordination polymers containing benzotriazolate based ligands,[13] the area of MOF type of compounds using benzobistriazolate as linkers as yet remained largely unexplored. Herein, we present a novel cubic MOF, "MFU-4", (MFU being the acronym for *M*etal-organic *F*ramework *U*lm University) $[Zn_5Cl_4(BBTA)_3]\cdot 3DMF$ (**1**), constructed from $\{Zn_5Cl_4\}^{6+}$ secondary building units (SBUs) interconnected with BBTA linkers. The incentive of using BBTA type of linkers came from our previous work on T_d symmetrical pentanuclear metal complexes of the type $[M'Zn_4Cl_4(L_6)]$, where M′ = Zn or Co(II), and L represents a 1,2,3-benzotriazolate ligand,[14] which indicated that similar structural building units might be employed for the construction of periodic cubic frameworks (Scheme 1).

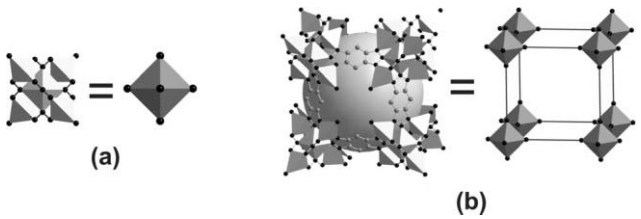

Scheme 1 Construction principle of cubic MFU-4-type frameworks (b) comprising T_d symmetric $\{Zn_5Cl_4\}^{6+}$ coordination units (a), linked by linear benzobistriazolate linkers (octahedrally coordinated Zn, light grey; C, dark grey; N and Cl, black). The grey sphere represents a larger cavity inside MFU-4 framework.

[a]*Ulm University, Institute of Inorganic Chemistry II - Materials and Catalysis, Albert-Einstein-Allee 11, D-89081, Ulm, Germany. E-mail: dirk.volkmer@uni-ulm.de; Fax: (+)49 (0)731 50-23039; Tel: (+)49 (0)731 50-23921*

[b]*Fachbereich Chemie, Philipps-Universität Marburg, Hans-Meerwein-Strasse, D-35043, Marburg, Germany*

[c]*Department of Inorganic Chemistry, Dresden University of Technology, Mommsenstr. 6, D-01069, Dresden, Germany*

† Electronic supplementary information (ESI) available: XRPD patterns, IR spectra, TGA curves, optical and SEM micrographs, crystallographic table from powder diffraction data, tables containing selected bond lengths. CCDC reference numbers 723714, 723715, and 723716 for **1**, high temperature structure of **1** obtained from powder diffraction data, and **2**, respectively. For ESI and crystallographic data in CIF or other electronic format see DOI: 10.1039/b904280f

Initial molecular mechanics investigations suggested that there should be exactly one way of assembling $\{Zn_5Cl_4\}^{6+}$ SBUs and $BBTA^{2-}$ dianions into a cubic lattice, assuming that all N-donor atoms of the BBTA ligands are coordinated with metal centers. Indeed, this working model proved to be correct leading to the directed solvothermal synthesis of compound **1** (MFU-4). However, in the course of comparative investigations on suitable preparation conditions we discovered that the yield of this compound is delicately dependent on the solvent used in synthesis. Thus, employing *N*,*N*′-dimethylacetamide (DMA) as solvent instead of *N*,*N*′-dimethylformamide (DMF), compound **2** crystallizes from the reaction mixture, which constitutes a densely packed 2D layered coordination polymer, in contrast to the porous cubic framework of **1**. The main difference between both structures is the coordination mode of the BBTA ligands: In contrast to compound **1** we found that only two (N^1 and N^3) of the triazolate N-donor atoms are coordinating to zinc ions in compound **2**. To the best of our knowledge **2** is the first example of a 2D coordination polymer containing BBTA ligand.

Microwave-assisted synthesis of inorganic materials has attracted much attention in recent years. This technique often leads to a rapid and efficient synthesis of porous materials within a few minutes,[15] instead of days of typical solvothermal routes, and, moreover, it offers phase selectivity[16] and facile control over crystal morphology.[17] This method has been successfully applied for the rapid synthesis of several well-known porous MOFs such as MOF-5, MIL-77, MIL-100, or MIL-101.[18] Encouraged by these facts, we have established an efficient microwave synthesis leading to compound **1** at very short reaction times (typically 10 min) with acceptable yields.

In this article, we present the syntheses, structural characterizations, as well as thermal, fluorescent, and sorption properties of the above mentioned novel coordination polymers.

Experimental

Materials and general methods

The H_2-BBTA ligand was synthesized as described previously.[19] All other starting materials were of reagent grade and used as received from the commercial supplier. Fourier transform infrared (FTIR) spectra were recorded from KBr pellets in the range 4000–400 cm^{-1} on a Bruker IFS FT-IR spectrometer. The following indications are used to characterize absorption bands: very strong (vs), strong (s), medium (m), weak (w), shoulder (sh), and broad (br). Elemental analyses (C, H, N) were carried out on a Perkin-Elmer 2400 Elemental Analyzer. Thermogravimetric analysis (TGA) was performed with a TGA/SDTA851 Mettler Toledo analyzer in a temperature range of 25–1100 °C in flowing nitrogen at a heating rate of 10 °C min^{-1}. TG-MS analysis was carried out using a STA 409 PC/PG-Luxx (Netzsch) simultaneous thermal analyzer coupled with QMS 403C-Aeolos Mass Spectrometer in a temperature range of 30–1100 °C under Ar atmosphere with a heating rate of 5 °C min^{-1}. Ambient temperature X-ray powder diffraction (XRPD) patterns were measured using a Philips X′Pert PRO powder diffractometer operated at 40 kV, 40 mA for Cu target ($\lambda = 1.5406$ Å) with a scan speed of 30 s $step^{-1}$ and a step size of 0.008°. Temperature-dependent X-ray powder diffraction measurements were performed in air with the same diffractometer equipped with an Anton Paar HTK 1200 N reaction chamber. The heating rate between two temperatures was 5 °C/min and once the corresponding temperature was reached, the sample was held at this temperature for 1 h before measuring the pattern. The simulated powder patterns were calculated using data from single crystal X-ray diffraction. Energy dispersive X-ray analysis (EDX) was performed on an EDAX (Phönix) X-ray detection system with 30 mm^2 SUTW window. SEM images were recorded using a Zeiss DSM 962 scanning electron microscope. The solid-state fluorescence emission spectra were collected on a SPEX Fluorolog II spectrofluorometer (Spex Industries, Edison, NJ) in the 320–750 nm region at room temperature using an excitation wavelength of 300 nm. Powder samples were enclosed between two microscope slides having a thickness of 0.2 mm each. The area occupied by the samples was *ca.* 5 mm × 5 mm. Solid state UV-vis spectra were recorded on an Analytik Jena Specord 50 UV-vis spectrometer in the range of 200–800 nm with a lamp change at 450 nm. The powder samples were applied as suspensions in Nujol, mounted between two quartz plates. The nitrogen and hydrogen sorption isotherms at −196 °C up to 1 bar were measured using a Quantachrome Autosorb-1C apparatus. High purity gases were used for the adsorption experiments (nitrogen 99.999%, hydrogen 99.999%). Water adsorption isotherms were measured with a Quantachrome Hydrosorb 1000 apparatus. Prior to the measurements, the samples were evacuated at 250 °C for 24 h. The amount of activated sample used for the adsorption measurements was 150 mg.

Safety note! Benzobistriazolate complexes are potentially explosive, and caution should be exercised when dealing with such derivatives. However, the small quantities used in this study were not found to present a hazard.

Syntheses

$[Zn_5Cl_4(BBTA)_3]\cdot 3DMF$ (1).

Solvothermal method. A mixture of anhydrous $ZnCl_2$ (136 mg, 1.00 mmol) and H_2-BBTA (40 mg, 0.25 mmol) was dissolved in 4 mL of DMF and the solution was placed in a glass tube (10 mL). The tube was sealed and heated at 140 °C for 3 days, then cooled to room temperature. The supernatant was removed and the remaining yellow microcrystalline solid was washed with DMF (3 × 1 mL) and dried in air to yield 62 mg (0.053 mmol, 27%, batch 1) of **1** as mostly cubic microcrystals along with very few octahedral microcrystals. Larger single crystals of X-ray quality were grown under slightly different reaction conditions (batch 2). A solution of anhydrous $ZnCl_2$ (51 mg, 0.37 mmol) and H_2-BBTA (20 mg, 0.12 mmol) in 2 mL of DMF was placed in a 10 mL glass tube, the tube was sealed and heated at 140 °C for 3 days, and then the mixture was cooled to room temperature to produce a mixture of X-ray quality, yellow octahedral crystals and smaller, yellow cubic microcrystals. A single crystal X-ray diffraction study was performed by selecting an octahedral crystal of dimensions 0.08 × 0.06 × 0.06 mm^3 from this mixture. The yield was 30 mg (0.026 mmol, 35%, batch 2). Crystals precipitated in both batches showed the same analytical results. Anal. Calcd for $C_{27}H_{27}Cl_4N_{21}O_3Zn_5$: C, 27.89 H, 2.34 N, 25.30. Found: C, 27.97 H, 2.82 N, 25.80%. IR (KBr, cm^{-1}): 3438 (br), 3080 (w), 2918 (w), 2848 (w), 2392 (br), 1652 (vs), 1487 (w), 1434 (w), 1408 (m),

1381 (m), 1310 (m), 1237 (w), 1200 (s), 1163 (sh), 1092 (m), 1056 (w), 862 (s), 659 (m), 569 (w), 469 (w), 425 (m).

Microwave irradiation method. A mixture of $ZnCl_2$ (68 mg, 0.49 mmol) and H_2-BBTA (20 mg, 0.12 mmol) in DMF (1 mL) was placed in a Pyrex sample tube (10 mL). The tube was sealed and placed in a microwave synthesizer (CEM, Discover S). The resulting mixture was heated to 155 °C at 300 W, kept under these conditions for 10 min and then cooled to room temperature. A yellow, cubic microcrystalline material (25 mg, 22%) was obtained by centrifugation, washing with DMF (3 × 1 mL) and drying in air at ambient conditions. This material exhibited the same analytical results as the one obtained by the solvothermal method.

[ZnCl(BBTA)$_{0.5}$(DMA)] (2). A mixture of anhydrous $ZnCl_2$ (51 mg, 0.37 mmol) and H_2-BBTA (20 mg, 0.12 mmol) was dissolved in 4 mL of DMA and the solution was placed in a glass tube (10 mL). The tube was sealed and heated at 120 °C for 3 days, then cooled to room temperature. The resulting colorless, block shaped crystals were collected by filtration, washed with DMA (3 × 1 mL) and dried in air to yield 30 mg of **2** (0.026 mmol, 35%). Anal. Calcd for $C_7H_{10}ClN_4OZn$: C, 31.48 H, 3.77 N, 20.98. Found: C, 31.62 H, 3.84 N, 21.08%. IR (KBr, cm^{-1}): 3409 (br), 3096 (w), 2972 (w), 2934 (w), 2783 (w), 2349 (w), 1606 (s), 1498 (w), 1421 (w), 1397 (m), 1298 (m), 1252 (w), 1168 (s), 1021 (m), 963 (w), 846 (s), 834 (sh), 744 (m), 620 (m), 602 (sh), 487 (m), 439 (w).

Structure determination

Structures of **1** and **2** were determined from single crystal data. The data of **1** were collected on a diffractometer equipped with a STOE imaging plate detector system IPDS 2T, using Mo Kα radiation with graphite monochromatization (λ = 0.71073 Å) at T = 103 K. Initial structures were solved by direct methods and refined by full-matrix least-squares techniques based on F^2 using SHELXS-97 and SHELXL-97 software.[20] Single crystal X-ray diffraction studies of compound **2** were performed on a STOE IPDS diffractometer employing monochromated Mo Kα radiation (λ = 0.71073). Initial structures were solved by direct methods and refined by full-matrix least-squares techniques based on F^2 using the SHELXL-97 program.[20] CCDC reference numbers 723714, 723715, and 723716 for **1**, high temperature structure of **1** obtained from powder diffraction data, and **2**, respectively.† Details of single crystal data collection and refinement of compounds **1** and **2** are summarised in Table 1.

Rietveld refinement

Initial TG analysis of **1** shows that the occluded guest DMF molecules can be removed at T < 350 °C. Therefore, the X-ray powder diffraction data collected at this temperature were used for a Rietveld structure refinement. The intention of this process was to check the thermal stability of the framework and to elucidate whether or not the occluded solvent molecules can be cleanly removed from the compound, without significant loss of crystallinity. In fact, it was possible to determine the crystal structure of the compound only from this data set, whereas any efforts of solving the crystal structure from VTXRPD data collected from a sample held at a temperature in the range from 30 to 300 °C were unsuccessful. In these cases, large discrepancies between experimental and calculated intensities with high, unacceptable R-values were observed. Moreover, the unit cell volume of **1** at 350 °C was slightly smaller than the corresponding unit cell volume from samples kept at lower temperature (Table S2, ESI†), suggesting that a slight shrinkage of the structure has taken place after removal of DMF molecules. The mechanism by which DMF molecules can be liberated from the cavities of compound **1** remains enigmatic however, since the very small pore aperture of the A-cells interconnecting the solvent-filled larger B-cells restricts the diffusion of DMF molecules across the crystal lattice at ambient conditions (Fig. 3, see later).

Lattice parameters of compound **1** at different temperatures were determined using the PROSZKI package.[21] Structure determination, independent from single crystal studies, was performed using the EXPO2004 package,[22] which combines a full pattern decomposition program (EXTRA) and a direct method program (SIR97) optimized for powder diffraction data. During pattern decomposition the lattice parameters were not refined. The whole crystal model, *i.e.* the zinc, chlorine, nitrogen and carbon atoms, was found using the direct method. The Rietveld refinement was carried out using the Jana2000 program.[23] Weak geometric restraints on bond distances were used during the refinement process. The preferred orientation was chosen along the [111] direction and it was refined applying the March-Dollase formula. The texture parameter was refined up to 0.74. The final Rietveld plot is presented in Fig. 1.

Table 1 Single crystal data and structure refinement parameters for compounds **1** and **2**

Compound	**1**	**2**
Formula	$C_{27}H_{27}Cl_4N_{21}O_3Zn_5$	$C_7H_{10}ClN_4OZn$
Formula mass	1162.35	267.01
T/K	103(2)	293(2)
λ/Å	0.71073	0.71073
Crystal dimensions/mm	0.08 × 0.06 × 0.06	0.15 × 0.23 × 0.23
Crystal system	Cubic	Monoclinic
Space group	*Fm*-3*m*	$P2_1/c$
a/Å	21.697(3)	9.812(2)
b/Å		8.6012(17)
c/Å		12.571(3)
β/°		96.91(3)
V/Å^3	10214(2)	1053.3(4)
Z	8	4
D_c/g cm^{-3}	1.482	2.071
μ/mm^{-1}	2.573	2.558
F(000)	4624	636
θ Range/°	4.60–26.77	2.88–25.95
Measured reflections	16467	11882
Independent reflections/R_{int}	542/0.1181	1920/0.1948
Data/restraints/parameters	542/0/48	1920/0/127
R_1 ($I > 2\sigma(I)$)[a]	0.0678	0.0576
wR_2 (all data)[b]	0.1514	0.1600
Goodness-of-fit on F^2	1.199	0.884
$\Delta\rho_{max, min}$/e Å^{-3}	0.977, –0.725	0.919, –0.760

[a] $R_1 = \sum\|F_o\| - |F_c\|/\sum|F_o|$. [b] $wR_2 = \{\sum[w(F_o^2 - F_c^2)^2]/\sum[w(F_o^2)^2]\}^{1/2}$.

Results and discussion

Syntheses and characterization

Though the role of the reactive solvent containing a hydrolytically unstable amide bond is similar for the synthesis of both

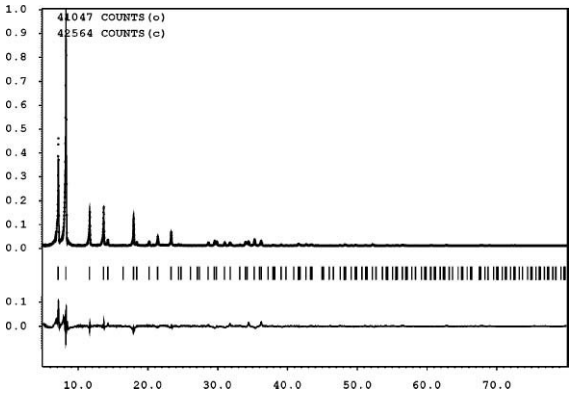

Fig. 1 Rietveld refinement plots for heat-treated compound **1**. Dotted and solid lines represent observed and calculated patterns, respectively with peak markers and the difference plot shown at the bottom. XRPD data were collected at 350 °C with a total heating period of 8 h.

compounds described in this manuscript, we have obtained two different coordination polymers using DMF (compound **1**) and DMA (compound **2**), respectively. Both compounds can be obtained starting from a variety of reaction mixtures with different ratios of $ZnCl_2/H_2$-BBTA (2:1, 3:1 and 4:1). However, **2** can be obtained in pure phase at 120 °C under solvothermal conditions while the solvothermal synthesis of **1** requires higher temperature (140 °C). To reduce the synthesis time from several days to only a few minutes, a microwave synthesis has been developed for **1**. Both compounds are stable in air, insoluble in water and in common organic solvents.

An EDX measurement performed on as-synthesized compound **1** by the solvothermal method shows that the relative ratio of Zn:Cl is 1:1.6, which closely matches the theoretical ratio (1:1.4).

A SEM image shows mostly cubic microcrystals with truncated corners, along with very few octahedral microcrystals having formed during the synthesis of compound **1** by the solvothermal method (Fig. 2). Crystals of similar shape, with a lower fraction of octahedral microcrystals, however, were obtained from microwave synthesis of **1** (Fig. S8, ESI†).

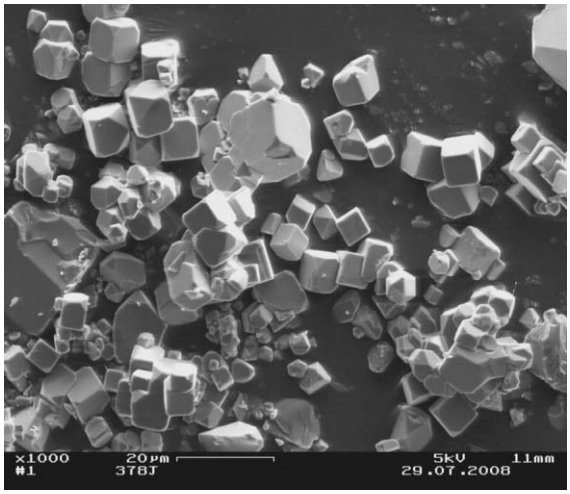

Fig. 2 SEM image of compound **1** (batch 1) prepared by the solvothermal method.

Structure description

The single crystal X-ray diffraction study reveals that **1** exhibits a cubic six-connected net (Fig. 3) which may be conceptually derived in two stages: first, the nodes (vertices) of the net are replaced by cationic pentanuclear $Zn_5Cl_4^{6+}$ coordination units; second, the links (edges) of the net are replaced by finite rods ('struts') of $BBTA^{2-}$ dianions.

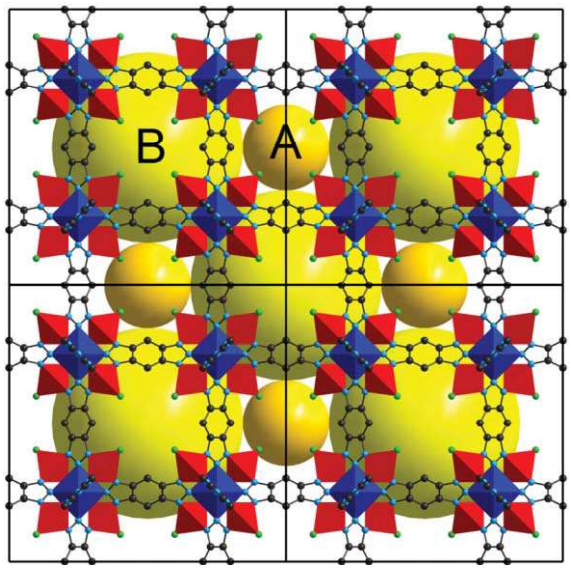

Fig. 3 Ball and stick representation of the MFU-4 framework along the crystallographic *a*-direction (octahedrally coordinated Zn: blue octahedra; tetrahedrally coordinated Zn, red tetrahedra; N, light blue; C, grey; Cl, green). All hydrogen atoms are removed for clarity. The larger, light yellow spheres represent the cavities of B-cells whereas the smaller, dark yellow spheres represent the cavities of A-cells.

In the pentanuclear coordination units, six BBTA ligands are monodentately coordinated to the central octahedrally coordinated Zn ion. The six BBTA ligands span a Cartesian coordinate system with the Cartesian axes running through the metal ion at the origin and the N^2 atoms of the coordinated ligands. The BBTA ligands are twisted around their coordinative bond to the central metal ion such that the nitrogen atoms are placed on the edges of an imaginary tetrahedron. At the corners of this tetrahedron are placed four additional Zn ions which are coordinated to three N donor atoms of the BBTA ligands and a chloride anion creating a distorted tetrahedral coordination environment. Each BBTA ligand shows a $\eta^3{:}\mu_6$ coordination motif similar to the coordination mode of discrete low-molecular Zn coordination compounds described previously.[13b,14] Furthermore, each Zn_5 unit is connected to six BBTA ligands by 18 Zn–N bonds, with each ligand coordinating one central and two peripheral Zn atoms. In compound **1**, the octahedrally coordinated Zn atom shows a Zn-N distance of 2.212(7) Å, and the tetrahedrally coordinated Zn atom shows a Zn-N distance of 2.046(6) Å (Table S4, ESI†). These values are in good agreement to other Zn triazolate complexes (1.98–2.05 Å for tetrahedral coordination, 2.14–2.22 Å for octahedral coordination).[24]

An estimation with the program PLATON/SQUEEZE[25] using the powder data of **1** kept at 350 °C reveals that the total potentially accessible void volume is 5372 $Å^3$ which is 53.1% of the unit cell

volume. By analogy to MOF-5,[26] the framework of **1** has two different types of cavities (the smaller and the larger ones are referred to as A and B cells, respectively) arranged in an alternating fashion (Fig. 3). A-cells are represented by the cubic arrangement of chloride ligands having a minimum non-bonding distance of 4.257(4) Å to each other. The centre of the A-cells has a distance of 3.68 Å to each Cl atom. The aperture joining the two structurally different cavities is built up by 4 Cl atoms at a distance from 3.01 Å from its geometric centre. Taking the van der Waals radii of Cl atoms (1.75 Å) into account, imaginary spheres with a diameter of 3.87 Å could fit into the A-cells (which roughly corresponds to the van der Waals diameter of Ar atoms), and the aperture would admit the passage of an imaginary sphere with a diameter of 2.52 Å. Each of the larger B-cells, on the other hand, is surrounded by twelve phenyl rings, and an imaginary sphere with a diameter of 11.94 Å would fit into it, taking the van der Waals radii of C atoms into account. Due to their very large volume the B-cells are filled with 6 DMF guest molecules each. These occluded solvent molecules are highly disordered thus it was impossible to refine their locations from the electron density distribution obtained from X-ray diffraction data. For consideration of the smeared electron density associated with the occluded DMF molecules, it was necessary to assign accordingly, partially occupied split positions for a total of three DMF molecules per asymmetric unit. The high mobility of the solvent within the B-cells is indicated by the fact that even reduction of the crystallographic symmetry did not serve to localize the $HC(O)N(CH_3)_2$ atomic sites.

Owing to the construction principle of MFU-4 (**1**) DMF molecules moving from one B-cell into another must pass through an A-cell. The small pore diameter of A-cells as well as the small aperture connecting the two types of cells severely restricts the transport of DMF molecules at ambient conditions. According to TG analysis, however, the occluded DMF molecules can be removed completely upon heat treatment (>250 °C) of **1** under high vacuum. This could, at least partially, be due to decomposition of DMF molecules at this temperature producing smaller molecular fragments which could pass through the A-cells. The existence of volatile DMF as well as its decomposition products, liberated by heating **1**, have been confirmed by TG-MS analysis (Fig. S10, ESI†). The $m/z = 73$ profile shows a signal at 226 °C and 244 °C, which can be assigned to the presence of DMF. Both $m/z = 44$ and $m/z = 30$ profiles exhibit signal at 234 °C due to the presence of dimethylamine and formaldehyde, respectively.

Compound **2** exhibits a 2-D layered framework (Fig. 4) crystallizing in a monoclinic crystal system, within space group $P2_1/c$. The 2D layers extend into the *yz*-plane of the crystallographic lattice while they are stacked along crystallographic *x*-direction. Each Zn centre is placed in a distorted tetrahedral coordination environment (Fig. 4a) consisting of one chloride ion, the O-donor atom stemming from a monodentately coordinated DMA molecule, and two N atoms from two different BBTA ligands with two different Zn-N distances: 1.992(6) and 1.995(5) Å (Table S5, ESI†). These values are in good agreement with other Zn triazolate complexes having tetrahedral zinc centers.[24] The two BBTA ligands are inclined with respect to each other. Each ligand exhibits a $\mu_{1,3}$-bridging coordination mode which was previously documented for other complexes containing Zn ions and benzotriazolate anions.[24b,c]

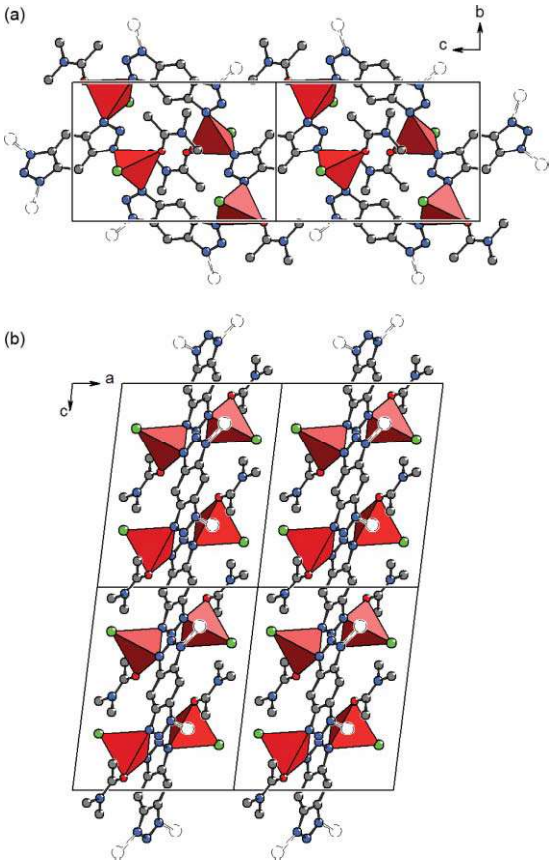

Fig. 4 Crystal packing diagrams of **2**. (a) Ball and stick representation of a single 2-D coordination polymer layer. (b) Same representation showing the stacking of adjacent 2-D layers of **2** along the crystallographic *a* direction. (Zn, red tetrahedra; N, light blue; C, grey; Cl, green). Zinc atoms located outside of the unit cell boundaries are displayed as broken spheres. Hydrogen atoms are omitted for clarity.

TGA and XRPD

Phase purity of **1** and **2** were examined using XRPD patterns recorded from compounds **1** and **2** at ambient conditions. Though it was impossible to get specimens of **1** containing 'only cubic' and 'only octahedral' crystal species, the simulated XRPD pattern obtained from single crystal X-ray diffraction data performed on an octahedral single crystal of **1** matches quite well with the experimental XRPD patterns (Fig. S1, ESI†) of specimens of **1** from both batch 1 (containing ~95% cubic crystals) and batch 2 (containing ~1:1 ratio of cubic and octahedral crystals), confirming that both cubic and octahedral crystals are identical phases with different habitus. The experimental XRPD patterns of **2** are also consistent with the simulated ones as gleaned from the single-crystal X-ray diffraction data (Fig. S2, ESI†). Moreover, TGA and variable temperature XRPD (VTXRPD) experiments were performed to examine the thermal stability of both compounds. It is observed that **2** decomposes above 200 °C while **1** decomposes above 350 °C indicating a very high thermal stability.

In the TG curve of **1** (Fig. 5a), the gradual weight loss of 17.8% in the range 120–300 °C is attributed to the removal of three DMF molecules per formula unit (calc. 18.8%), which is consistent with the results from elemental analysis. No further weight loss is

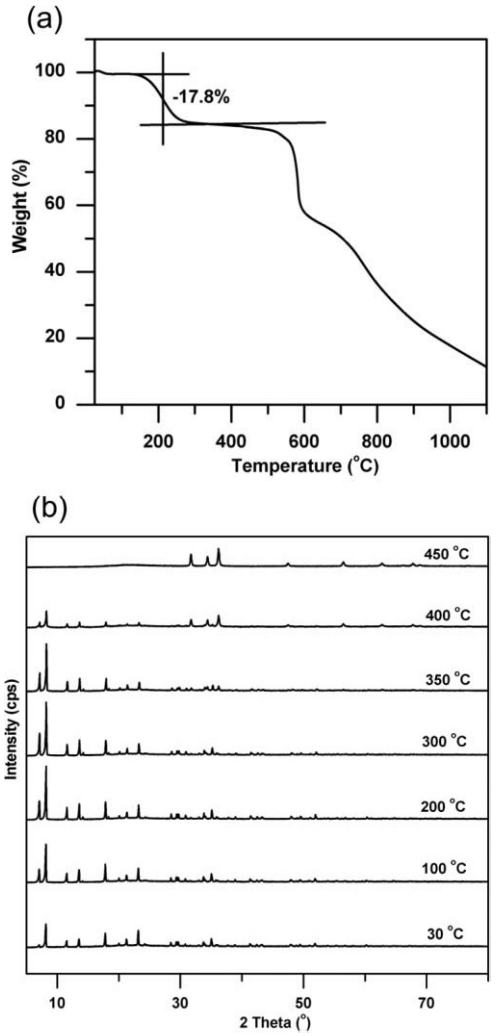

Fig. 5 (a) Thermogravimetric analysis of **1** under nitrogen atmosphere; (b) VTXRPD plots of **1** in the range of 30–450 °C.

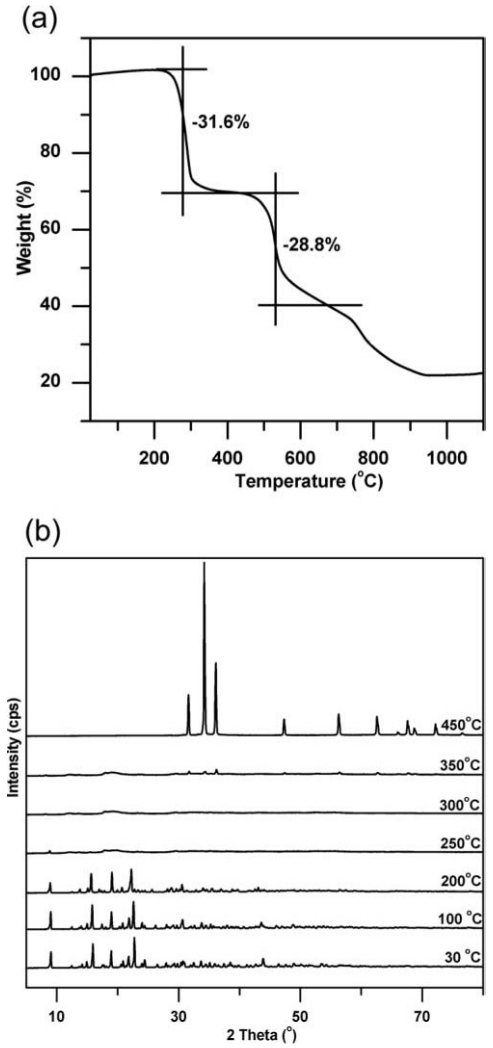

Fig. 6 (a) Thermogravimetric analysis of **2** under nitrogen atmosphere; (b) VTXRPD plots of **2** in the range of 30–450 °C.

observed until 400 °C, when the framework starts to decompose leading to ZnO.

Variable temperature X-ray powder diffraction (VTXRPD) studies (Fig. 5b) show that **1** is stable up to 350 °C and crystallinity is retained upon the loss of free DMF molecules. In the temperature range 350–400 °C, ZnO appears as new crystal phase which predominates above 450 °C, when the framework has completely decomposed.

In the TG curve of **2** (Fig. 6a), three weight loss steps are observed. The first weight loss of 31.6% in the range 150–300 °C is attributed to the loss of one coordinated DMA molecule per formula unit (cald. 32.6%). The second weight loss of 28.8% in the range of 400–650 °C is due to the removal of 0.5 molecule of coordinated BBTA ligand per formula unit (cald. 29.6%), suggesting that compound **2** starts to decompose in this temperature region. The third weight loss step is also due to the decomposition of the compound leading to formation of ZnO.

From the variable temperature XRPD patterns (Fig. 6b), it becomes obvious that **2** is stable only up to 200 °C. After that the compound starts to decompose giving rise to an amorphous phase which persists until 350 °C. Above 350 °C, first signs of formation of crystalline ZnO appear, and above 450 °C, the amorphous phase has completely disappeared, leading exclusively to crystalline ZnO.

Luminescence and UV-vis spectroscopy

Inspired by the strong fluorescence emissions of previously reported coordination polymers[24b,c] and MOFs[13b] containing zinc and benzotriazolates, we investigated the luminescent properties of **1** and **2**. As shown in Fig. 7a, free H_2-BBTA exhibits a broad fluorescence emission band centered at ~550 nm upon excitation at a wavelength of 300 nm. Because the emission band of **1** is similar to that of the free H_2-BBTA ligand, it should be assigned to the intraligand π–π* transition of the BBTA ligand. A broad band of this kind is also observed in the fluorescence emission spectrum of **2**, however with a significant blue-shift. In addition, **2** shows some sharp emission bands at 390, 400, 420, and 445 nm which may be assigned to charge transfer between the deprotonated BBTA ligand and the zinc ions.

The solid-state UV-vis spectra of free H_2-BBTA ligand displays two weak absorption peaks at 255 and 295 nm in the UV region, as depicted in Fig. 7b. The coordinated BBTA ligand in both **1** and **2**, also exhibit weak absorption peaks at the same positions.

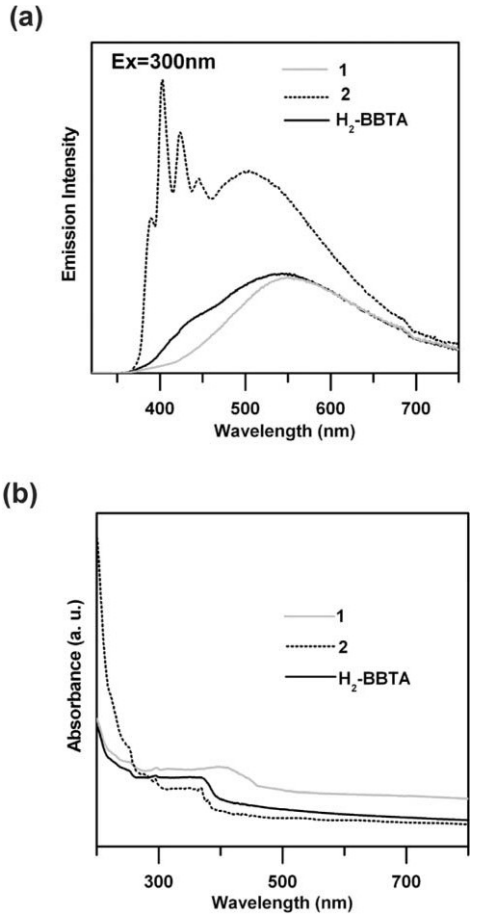

Fig. 7 (a) Solid-state photoluminescence spectra for **1**, **2**, and free H_2-BBTA ligand. (b) Solid-state UV-vis spectra for the same compounds.

In addition, both **1** and free H_2-BBTA show one broad absorption band at 410 and 370 nm, respectively. Compound **2**, on the other hand, shows two additional weak, sharp absorption peaks at 370 and 380 nm.

Physisorption results

Nitrogen, hydrogen and water adsorption studies were performed on compound **1**. The nitrogen adsorption measurement revealed that the compound adsorbs almost no nitrogen at –196 °C and pressure up to 1 bar. Therefore, the specific surface area and pore volume could not be determined from the nitrogen adsorption experiment, as it is routinely done for the characterization of porous materials. However, a surface area calculated from a Monte Carlo integration technique, where the probe molecule is "rolled" over the framework inner surface as described by Düren *et al.*[27] predicts an accessible surface area as high as 1611 m^2g^{-1} indicating that MFU-4 should possess a porous framework.

This permanent porosity could be proven using hydrogen adsorption revealing a remarkable accessible inner pore volume. The hydrogen adsorption isotherm follows type I behaviour and the maximum uptake achieved at –196 °C and 1 bar is 1.62 wt.% (Fig. 8). The selective adsorption of hydrogen over nitrogen at –196 °C is rare and has been previously demonstrated only for few MOFs with short linkers.[28] The "sieving effect" in these compounds can be attributed to the small aperture of the pores.

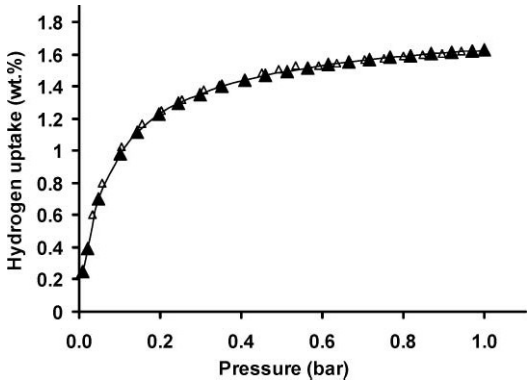

Fig. 8 Hydrogen adsorption (solid symbols) and desorption (empty symbols) isotherms measured for MFU-4 at –196 °C up to 1 bar.

The permanent porosity of **1** has been confirmed by water adsorption measurements at 25 °C. The kinetic diameter of water (0.265 nm) is even smaller than that of hydrogen (0.289 nm) which leads to the assumption that water should also be adsorbed on MFU-4.

As depicted in Fig. 9, the water adsorption shows a steep uptake in the region from $p/p_0 = 0.1$ up to 0.35, following saturation. The pore volume estimated from the water adsorption isotherm at $p/p_0 = 0.9$ is 0.42 $cm^3\ g^{-1}$. It should be noted that the estimation of micropore volume using a water vapor adsorption isotherm often yields slightly different (usually underestimated) values as compared to adsorption data using other probe molecules (such as nitrogen or argon). In case of water, the hydrophobic-hydrophilic properties of the surface govern the adsorption process and the adsorptive itself strongly interacts *via* hydrogen bonds leading to adsorption phenomena different from nitrogen adsorption experiments.[29]

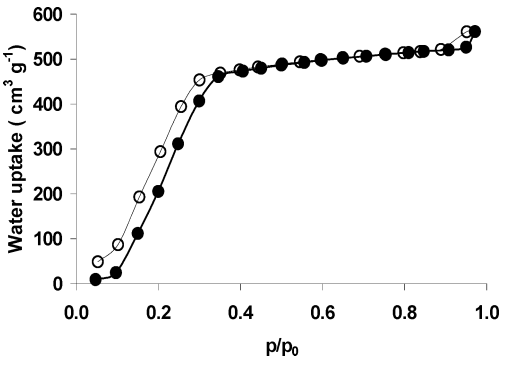

Fig. 9 Water adsorption (solid symbols) and desorption (empty symbols) isotherm measured for compound **1** at 25 °C.

The water adsorption measurement was repeated two times on the same sample. Between the measurements the sample was evacuated at 250 °C for 24 hours. The exactly reproducible nature of the isotherm points at the high stability of the framework against moisture. The combination of molecular sieving characteristics and moisture stability suggests using MFU-4 in gas separation processes where hydrogen molecules (or similarly: helium atoms) have to be separated from mixture of gases (*e.g.* CO_2, CO, O_2 or N_2).

Conclusions

We have successfully prepared and fully characterized an unprecedented cubic framework (compound **1**, MFU-4), constructed from $BBTA^{2-}$ dianions and $Zn_5Cl_4^{6+}$ coordination units. Compared to the solvothermal synthesis, the preparation of **1** by microwave irradiation leads to a large reduction in reaction time. A different coordination mode of the benzobistriazolate ligands has been established by the synthesis and characterization of coordination polymer **2**, which demonstrates that the particular choice of solvent plays a crucial role in the synthesis of crystalline phases of coordination polymers of similar composition, especially MOFs. Thermogravimetric analysis indicates that MFU-4 possesses a slightly higher thermal stability (350 °C) than MOF-5. Strong luminescence exhibited by these novel coordination polymers suggests that they might be excellent candidates for photoactive material.

The crystal lattice of MFU-4 resembles MOF-5 in terms of structural parameters as both are cubic, and both possess two different types of cavities. However, the coordination unit of MFU-4 framework differs from MOF-5 (Scheme 2) with regard to the fact that MFU-4 contains zinc ions within different coordination environments (one octahedral and four tetrahedral metal centres) while MOF-5 has only tetrahedral zinc centres. As evidenced by our previous work on low-molecular homo- and heteropentanuclear complexes bearing structurally similar $\{MZn_4Cl_4\}^{6+}$ cores (M = Zn(II) or Co(II)),[14] replacement of the octahedrally coordinated zinc centers in MFU-4 by redox-active 3d or 4d transition metal ions should be feasible without affecting the framework structure, a non-trivial task which has remained elusive for MOF-5 type compounds so far.[30] Such heterometallic MFU-4 type frameworks could be useful in catalytic redox reactions provided that a facile synthesis for an extended benzobistriazolate ligand could be developed which allows for free diffusion of molecules in the voids of the constituting framework lattice.

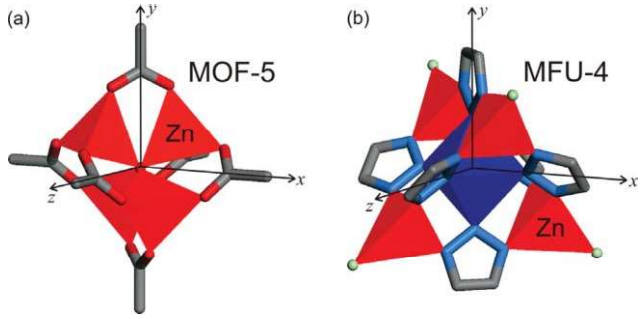

Scheme 2 Structural differences between coordination units in (a) MOF-5, and (b) MFU-4 (octahedrally coordinated Zn: blue octahedron; tetrahedrally coordinated Zn, red tetrahedra; N, light blue; C, grey; Cl, green).

Acknowledgements

Financial support by the DFG (Priority Program SPP 1362 "Porous Metal–Organic Frameworks") is gratefully acknowledged. The authors thank Dr Carlheinz Röcker (Institute of Biophysics, Ulm University) for help with the fluorescence studies.

References

1 (*a*) G. Férey, *Chem. Soc. Rev.*, 2008, **37**, 191; (*b*) A. J. Blake, N. R. Champness, P. Hubberstey, W. S. Li, M. A. Withersby and M. Schröder, *Coord. Chem. Rev.*, 1999, **183**, 117.
2 (*a*) G. Férey, *Nat. Mater.*, 2003, **2**, 136; (*b*) D. Maspoch, D. Ruiz-Molina and J. Veciana, *J. Mater. Chem.*, 2004, **14**, 2713; (*c*) G. J. Halder, C. J. Kepert, B. Moubaraki, K. S. Murray and J. D. Cashion, *Science*, 2002, **298**, 1762.
3 (*a*) F. Serpaggi, G. Férey and E. Antic-Fidancev, *J. Solid State Chem.*, 1999, **148**, 347; (*b*) F. Millange, C. Serre, J. Marrot, N. Gardant, F. Pellé and G. Férey, *J. Mater. Chem.*, 2004, **14**, 642.
4 (*a*) P. M. Forster, J. Eckert, J. S. Chang, S.-E. Park, G. Férey and A. K. Cheetham, *J. Am. Chem. Soc.*, 2003, **125**, 1309; (*b*) N. L. Rosi, J. Eckert, M. Eddaoudi, D. T. Vodak, J. Kim, M. O'Keeffe and O. M. Yaghi, *Science*, 2003, **300**, 1127; (*c*) G. Férey, M. Latroche, C. Serre, F. Millange, T. Loiseau and A. Percheron-Guégan, *Chem. Commun.*, 2003, 2976.
5 (*a*) F. Schüth and K. S. W. Sing, in *Handbook of Porous Solids*, Wiley-VCH, Weinheim, 2002; (*b*) M. J. Rosseinsky, *Microporous Mesoporous Mater.*, 2004, **73**, 15; (*c*) R. Q. Snurr, J. T. Hupp and S. T. Nguyen, *AIChE J.*, 2004, **50**, 1090.
6 T. Y. Shvareva, S. Skanthakumar, L. Soderholm, A. Clearfield and T. E. Albrecht-Schmitt, *Chem. Mater.*, 2007, **19**, 132.
7 (*a*) N. Guillou, Q. Gao, P. M. Forster, J. S. Chang, M. Noguès, S.-E. Park, G. Férey and A. K. Cheetham, *Angew. Chem., Int. Ed.*, 2001, **40**, 2831; (*b*) J. S. Seo, D. Whang, H. Lee, S. I. Jun, J. Oh, Y. J. Jeon and K. Kim, *Nature*, 2000, **404**, 982; (*c*) A. Corma, *J. Catal.*, 2003, **216**, 298.
8 (*a*) O. M. Yaghi, M. O'Keeffe, N. W. Ockwig, H.-K. Chae, M. Eddaoudi and J. Kim, *Nature*, 2003, **423**, 705; (*b*) J. L. C. Rowsell and O. M. Yaghi, *Microporous Mesoporous Mater.*, 2004, **73**, 3; (*c*) M. Eddaoudi, D. B. Moler, H. Li, B. Chen, T. M. Reineke, M. O'Keeffe and O. M. Yaghi, *Acc. Chem. Res.*, 2001, **34**, 319.
9 X. Zhao, B. Xiao, A. J. Fletcher, K. M. Thomas, D. Bradshaw and M. J. Rosseinsky, *Science*, 2004, **306**, 1012.
10 (*a*) H. J. Choi, M. Dincă and J. R. Long, *J. Am. Chem. Soc.*, 2008, **130**, 7848; (*b*) L. Hou, Y.-Y. Lin and X.-M. Chen, *Inorg. Chem.*, 2008, **47**, 1346.
11 (*a*) A. B. Lysenko, E. V. Govor, H. Krautscheid and K. V. Domasevitch, *Dalton Trans.*, 2006, 3772; (*b*) G. Yang and R. G. Raptis, *Chem. Commun.*, 2004, 2058; (*c*) C. Yang, X. Wang and M. A Omary, *J. Am. Chem. Soc.*, 2007, **129**, 15454; (*d*) C.-Y. Su, A. M. Goforth, M. D. Smith, P. J. Pellechia and H.-C. zur Loye, *J. Am. Chem. Soc.*, 2004, **126**, 3576; (*e*) W. Ouellette, M. H. Yu, C. J. O'Connor, D. Hagrman and J. Zubieta, *Angew. Chem., Int. Ed.*, 2006, **45**, 3497.
12 (*a*) M. Dincă, A. F. Yu and J. R. Long, *J. Am. Chem. Soc.*, 2006, **128**, 8904; (*b*) M. Dincă, A. Dailly, Y. Liu, C. M. Brown, D. A. Neumann and J. R. Long, *J. Am. Chem. Soc.*, 2006, **128**, 16876; (*c*) M. Dincă, W. S. Han, Y. Liu, A. Dailly, C. M. Brown and J. R. Long, *Angew. Chem., Int. Ed.*, 2007, **46**, 1419.
13 (*a*) X.-M. Zhang, Z.-M. Hao, W.-X. Zhang and X.-M. Chen, *Angew. Chem.*, 2007, **119**, 3526; (*b*) Y.-Y. Qin, J. Zhang, Z.-J. Li, L. Zhang, X.-Y. Cao and Y.-G. Yao, *Chem. Commun.*, 2008, 2532.
14 S. Biswas, M. Tonigold and D. Volkmer, *Z. Anorg. Allg. Chem.*, 2008, **634**, 2532.
15 S. H. Jhung, J. W. Yoon, J.-S. Hwang, A. K. Cheetham and J.-S. Chang, *Chem. Mater.*, 2005, **17**, 4455.
16 S. H. Jhung, J.-S. Chang, J.-S. Hwang and S.-E. Park, *Microporous Mesoporous Mater.*, 2003, **64**, 33.
17 Y. K. Hwang, J.-S. Chang, S.-E. Park, D. S. Kim, U. K. Kwon, S. H. Jhung, J.-S. Hwang and M. S. Park, *Angew. Chem., Int. Ed.*, 2005, **45**, 556.
18 J. Y. Choi, J. Kim, S. H. Jhung, H.-K. Kim, J.-S. Chang and H. K. Chae, *Bull. Korean Chem. Soc.*, 2006, **27**, 1523.
19 (*a*) H. Hart and D. Ok, *J. Org. Chem.*, 1986, **51**, 979; (*b*) M. D. Coburn and J. K. Berlin, *Synthesis*, 1974, 869; (*c*) J. H. Boyer and R. S. Buriks, *Organic Syntheses*, Wiley, New York, 1973, Collect. Vol. V, p 1067.
20 G. M. Sheldrick, *SHELXTL 5.1*, Bruker AXS Inc., 6300 Enterprise Lane, Madison, WI 53719-1173, USA, 1997.
21 W. Łasocha and K. Lewinski, *J. Appl. Crystallogr.*, 1994, **27**, 437.
22 A. Altomare, M. C. Burla, M. Camalli, B. Carrozzini, L. Cascarano, C. Giacovazzo, A. Guagliardi, A. G. G. Moliterni, G. Polidori and R. Rizzi, *J. Appl. Crystallogr.*, 1999, **32**, 339.
23 V. Petricek, M. Dusek and L. Palatinus, Jana2000, *The crystallographic computing system*, Institute of Physics, Praha, Czech Republic, 2000.

24 (*a*) I. Sotofte and K. Nielsen, *Acta Chem. Scand., Ser. A*, 1981, **35**, 739; (*b*) R.-F. Hu, J. Zhang, Y. Kang and Y.-G. Yao, *Inorg. Chem. Commun.*, 2005, **8**, 828; (*c*) J. Lu, K. Zhao, Q.-R. Fang, J.-Q. Xu, J.-H. Yu, X. Zhang, H.-Y. Bie and T.-G. Wang, *Cryst. Growth Des.*, 2005, **5**, 1091; (*d*) W. S. Sheldrick and P. Bell, *Z. Naturforsch., B: Anorg. Chem. Org. Chem.*, 1986, **41**, 1117; (*e*) X. Meng, Y. Song, H. Hou, Y. Fan, G. Li and Y. Zhu, *Inorg. Chem.*, 2003, **42**, 1306; (*f*) F. Jian, H. Xiao and P. Sun, *Acta Crystallogr., Sect. E: Struct. Rep. Online*, 2004, **60**, m38; (*g*) Z. An, H. Sun and R.-S. Wang, *Acta Crystallogr., Sect. E: Struct. Rep. Online*, 2005, **61**, m-2157.
25 A. L. Spek, *J. Appl. Crystallogr.*, 2003, **36**, 7.
26 (*a*) H. Li, M. Eddaoudi, M. O'Keeffe and O. M. Yaghi, *Nature*, 1999, **402**, 276; (*b*) S. Amirjalayer, M. Tafipolsky and R. Schmid, *Angew. Chem., Int. Ed.*, 2007, **46**, 463.
27 T. Düren, F. Millange, G. Ferey, K. S. Walton and R. Q. Snurr, *J. Phys. Chem. C*, 2007, **111**, 15350.
28 (*a*) D. N. Dybtsev, H. Chun, S. H. Yoon, D. Kim and K. Kim, *J. Am. Chem. Soc.*, 2004, **126**, 32; (*b*) S. Ma, X.-S. Wang, C. D. Collier, E. S. Manis and H.-C. Zhou, *Inorg. Chem.*, 2007, **46**, 8499; (*c*) J. Luo, H. Xu, Y. Liu, Y. Zhao, L. L. Daemen, C. Brown, T. V. Timofeeva, S. Ma and H.-C. Zhou, *J. Am. Chem. Soc.*, 2008, **130**, 9627; (*d*) S. Ma, X.-S. Wang, D. Yuan and H.-C. Zhou, *Angew. Chem.*, 2008, **120**, 4198.
29 P. Küsgens, M. Rose, I. Senkovska, H. Fröde, A. Henschel, S. Siegle and S. Kaskel, *Microporous Mesoporous Mater.*, 2009, **120**, 325.
30 Y. Wang, B. Bredenkötter, B. Rieger and D. Volkmer, *Dalton Trans.*, 2007, 689.